

Cite this: *RSC Sustainability*, 2023, 1, 2296

# Elucidating multiple reaction pathways for the degradation of antibiotics in water by a self-active single-atom zinc catalyst on biochar†

Jieming Yuan,<sup>a</sup> Yunkyong Han,<sup>a</sup> Krishnamoorthy Sathiyar,<sup>b</sup> Virender K. Sharma,<sup>b\*</sup> Abdol Hadi Mokarizadeh,<sup>c</sup> Mesfin Tsigie,<sup>c</sup> Jiechao Jiang<sup>d</sup> and Xingmao Ma<sup>b\*</sup>

Single-atom catalysts (SACs) have gained notable attention for the degradation of organic contaminants in water. However, most previous studies focused on the activation of peroxymonosulfate (PMS) or peroxydisulfate (PDS) for contaminant removal. Herein, we demonstrated for the first time that a Zn single-atom catalyst supported on biochar (SAZn@BC) alone removed ~98.0% of trimethoprim (TMP) within 30 minutes. The catalyst was synthesized via a simple pyrolysis process using oak wood powder as the feedstock. Detailed characterization of the catalyst demonstrated the single-atom Zn<sup>2+</sup> valence state and the Zn–N<sub>4</sub> local coordination structure, as well as abundant redox active oxygen functional groups on biochar. The coordination between Zn single atoms and the oxygen functional groups resulted in multiple reaction pathways for TMP degradation, including both reactive oxygen species-enabled degradation and direct oxidation. The Zn single atom in SAZn@BC was a necessary electron shuttling bridge for both pathways. Density functional theory (DFT) calculations supported the spontaneous occurrence of the proposed reactions in the system. Overall, our results showed that SAZn@BC alone can be a promising catalyst for a healthy and sustainable environment by removing contaminants in water effectively without any chemical or light energy input.

Received 2nd August 2023  
Accepted 16th October 2023

DOI: 10.1039/d3su00265a

rsc.li/rscsu

## Sustainability spotlight

Providing adequate accessible clean water is one of the key sustainable development goals of the United Nations due to the widespread water pollution. Catalytic degradation of environmental pollutants has played a significant role in addressing the water pollution challenge. As a novel class of catalytic materials, single-atom metal catalysts have attracted particularly high attention. However, traditional application of single-atom catalysts in water treatment generally relies on the activation of peroxymonosulfate (PMS) or peroxydisulfate (PDS) to achieve effective degradation, which increases the cost and complexity of the treatment process and is limited to water having low pH (<8.0). The development of cost-effective and simplified catalytic processes for effective contaminant degradation remains a pressing need. In this study, a self-active single-atom Zn catalyst supported on biochar (SAZn@BC) was synthesized, which demonstrated efficient degradation of a common antibiotic via co-occurring radical reactions and direct oxidation without the need for additional oxidants or energy input. The cost-effectiveness of SAZn@BC, coupled with its facile regeneration, renders it an exceptionally promising and sustainable material for a more economical and simplified water treatment process, which is critical for a large global population whose health is threatened by prevalent water contamination.

## 1. Introduction

The last few decades have witnessed extensive progress in the use of metal-based nanocatalysts for contaminant removal from water.<sup>1,2</sup> However, metal nanoparticle aggregation and possible metal ion leaching hindered their broad applications.<sup>3</sup> The emergence of single-atom catalysts (SACs) introduced a new class of materials that contain atomically dispersed metal sites and display remarkable performance in contaminant degradation due to their maximum metal utilization efficiency and excellent stability and selectivity.<sup>4,5</sup> The catalytic degradation of organic contaminants by SACs is generally achieved via the activation of peroxymonosulfate or peroxydisulfate.<sup>6</sup> However, they are relatively expensive and unstable at high temperature

<sup>a</sup>Department of Civil and Environmental Engineering, Texas A&M University, College Station, TX 77843, USA. E-mail: vsharma@tamu.edu

<sup>b</sup>Department of Environmental and Occupational Health, Texas A&M University, College Station, TX 77843, USA. E-mail: xma@civil.tamu.edu

<sup>c</sup>Department of Polymer Science and Polymer Engineering, University of Akron, Akron, OH 44325, USA

<sup>d</sup>Department of Materials Science & Engineering, University of Texas at Arlington, Arlington, TX 76019, USA

† Electronic supplementary information (ESI) available: Chemical materials and measurement procedures and results of superoxide radicals and hydrogen peroxide measurements, degradation products and MS1 and MS2 spectra of possible trimethoprim degradation metabolites, and setup of DFT calculations, TMP degradation with regenerated SAZn@BC, and TMP removal in the presence of different inorganic anions. See DOI: <https://doi.org/10.1039/d3su00265a>



or under light irradiation.<sup>7</sup> In addition, their activation is only effective in the pH range of 2.0–8.0.<sup>8</sup> Studies have also explored light irradiation to strengthen the catalytic activity of SACs. However, the light-mediated process requires a strong light source and adds cost and complexity.<sup>9</sup> Direct catalytic degradation of environmental contaminants by SACs without any extra oxidant or energy input is much needed. In the current paper, we have demonstrated for the first time the enhancement of the SAC catalytic activity by taking advantage of the unique features of support materials.

Biochar produced from waste biomass can be a promising support material for SACs because of its high specific surface area, tunable surface properties, excellent electrical conductivity, and low cost.<sup>10,11</sup> Numerous oxygen functional groups on biochar can potentially function as an electron reservoir to replace external sources.<sup>11</sup> Furthermore, biochar produced at high temperatures ( $T > 800$  °C) contains abundant defects that provide ideal anchoring sites for single-atom metals.<sup>11</sup>

Transition metals are commonly used in SACs, however, they are rare in the earth's crust and are expensive. Zinc (Zn) is the fourth most produced metal in the world. A N-doped carbon-supported Zn SAC was reported to have an excellent performance in CO<sub>2</sub> reduction.<sup>12</sup> It also has a more stable electronic structure because of the completely filled d orbital,<sup>13</sup> leading to an excellent performance in harsh environments. However, the potential of Zn SAC in environmental remediation is rarely explored.

Recently, the pervasiveness of antibiotics and the development of antibiotic resistance in water have caused serious concerns.<sup>14</sup> Trimethoprim (TMP) is a frequently detected antibiotic in natural water bodies with a reported concentration of up to 0.48 mg L<sup>-1</sup>.<sup>15</sup> A previous study showed that only 22.5% of orally taken TMP is metabolized in the human body and typical wastewater treatment plants remove less than 10% of TMP,<sup>16</sup> resulting in an average concentration of 2 mg L<sup>-1</sup> of TMP in wastewater effluents.<sup>15</sup> Thus, TMP is selected as a representative contaminant. Our objectives for this study were two-fold: (1) develop a simple and economical method to produce a Zn single-atom catalyst supported on biochar (SAZn@BC) and (2) investigate the mechanisms of SAZn@BC facilitated degradation of TMP.

## 2. Materials and methods

### 2.1. Materials

Detailed information on the sources and purity of chemicals used in this study are provided in the ESI (Text S1†). All chemicals were used as received.

### 2.2. Synthesis of a single-atom Zn catalyst on a biochar support (SAZn@BC)

Oak wood powder ground from wood pellets in a mortar was used as the biochar feedstock. For synthesizing the biochar, 10.0 g of wood powder, 5.0 g of dicyandiamide, and 0.29 g of zinc nitrate (resulting in about 1 wt% Zn by weight in the final product) were mixed with 150 mL of ultrapure water at 500 rpm

and 90 °C for one hour. 1 wt% Zn loading rate was chosen based on our preliminary data (Fig. S1†). The mixture was then dried in an oven at 85 °C for 20 hours before pyrolysis. The pyrolysis was carried out in a box furnace (Fisher Scientific, USA) for three hours with a continuous flow of nitrogen gas. The peak temperature was set at 800 °C, with a heating rate of 5 °C min<sup>-1</sup>. The product was ground into fine powder in a mortar and was acid washed with 100 mL of 2.0 M HCl with a stirring speed of 400 rpm for 2.0 hours at 90 °C on a magnetic stirrer. The product was then collected by vacuum filtration through a 0.45 μm membrane and washed with 2.0 L ultrapure water. The collected SAZn@BC was air-dried in a hood for 12 hours and ground with a pestle and mortar into fine powder before storage. SAZn@BC with 0 wt% Zn loading was also prepared with the same method and was named BC. The final product had a particle size ranging from 0.5 μm to 8.7 μm, with an average size of about 2.8 μm. The most dominant sizes were less than 3 μm.

### 2.3. Characterization of the single-atom Zn catalyst on biochar

The crystal structure of SAZn@BC was determined using X-ray diffraction (XRD, Bruker-AXS D8, Billerica, USA) with an X-ray source produced by a 2.0 kW Cu X-ray tube ( $\lambda = 1.5418$  Å). The XRD was operated at 40 kV and 25 mA. The morphology of the catalyst was determined by transmission electron microscopy (TEM, Titan Themis 300 S/TEM, Hillsboro, USA) at 300 kV. A high-angle annular dark field (HAADF) detector was applied to identify single Zn atoms, and a Super-X EDS detector was used to map the distribution of C, N, O, and Zn elements on SAZn@BC. X-ray photoelectron spectroscopy (XPS) analysis in a Phi 560 ESCA/SAM system (PerkinElmer, Waltham, MA, USA) was conducted to determine the oxygen-containing functional groups. Survey scans were performed in the 0–1200 eV range in 0.2 eV steps, while high-resolution XPS spectra for C, N, O, and Zn were acquired in 0.1 eV steps. X-ray absorption spectroscopy (XAS) was used to confirm the single-atom state of Zn and the local coordination structure. The XAS spectra were measured in transmission mode at the Materials Research Collaborative Access Team (MRCAT) sector 10 bending magnet beamline at Argonne National Laboratory's Advanced Photon Source using a double crystal detuned, water-cooled Si (111) monochromator in continuous scan mode. The data were processed and fitted using the IFEFFIT-based Athena and Artemis software packages.<sup>17</sup>

### 2.4. Degradation of trimethoprim (TMP)

The initial concentration of TMP was 10.0 μM, and the initial concentration of SAZn@BC was 0.20–0.4 g L<sup>-1</sup>. The study was carried out in 50.0 mL plastic tubes covered with aluminum foil and mixed on a shaker table at 300 rpm and 25 °C. One mL sample was withdrawn from each tube at different time intervals ( $t = 0, 0.5, 1.0, 2.0, 4.0, 7.0, 10.0$  hours) and was immediately filtered with a 0.45 μm syringe filter. The concentration of TMP was measured using a Dionex UltiMate 3000 high-performance liquid chromatography (HPLC) instrument



(Sunnyvale, USA). The total organic carbon (TOC) before and after 10 hours of TMP degradation was measured using a Shimadzu TOC analyzer in systems containing SAZn@BC. The impact of dissolved oxygen on TMP degradation was investigated by purging the mixture with purified N<sub>2</sub> gas for 0, 2, 5 and 10 minutes before TMP degradation, resulting in an oxygen level of 1.86–7.52 mg L<sup>-1</sup> in different reactors.

### 2.5. Quenching study

Three quenchers: 10.0 mM L-His, 0.5 M MeOH, and 50 U mL<sup>-1</sup> SOD (superoxide dismutase) were used to quench singlet oxygen (<sup>1</sup>O<sub>2</sub>), hydroxyl radical (<sup>•</sup>OH) and superoxide radical (O<sub>2</sub><sup>•-</sup>), respectively. TMP degradation by SAZn@BC was also performed in heavy water (D<sub>2</sub>O) to confirm the possible role of <sup>1</sup>O<sub>2</sub>. O<sub>2</sub><sup>•-</sup> and hydrogen peroxide (H<sub>2</sub>O<sub>2</sub>) were analyzed following methods reported in the literature,<sup>18,19</sup> which are summarized in Text S2.†

### 2.6. Electrochemical measurements

A three-electrode system (CH Instruments) with a 3.0 mm glassy carbon electrode as the working electrode, Ag/AgCl (3.0 M KCl) as the reference electrode and graphite rod as the counter electrode was used. Electrochemical impedance spectroscopy (EIS) was performed with open circuit voltage (OCV) as the specific voltage and an AC amplitude of 5.0 mV over the frequency range from 10<sup>5</sup> Hz to 0.01 Hz. The chronoamperometry *I*-*t* curve was measured by fixing OCV. The catalytic current was monitored by adding 1.0 mL of TMP (5.0, 10.0, and 20.0 μM) or oxygen-saturated water (0.5, 1.0 and 2.0 mL) into suspensions containing 10.0 mL deoxygenated water and 5.0 mg SAZn@BC or BC, with stirring at 300 rpm. In addition, the change in open circuit potential (OCP) was measured by adding 1 mL of contaminant (20 μM) solutions into SAZn@BC suspensions to determine the direct electron transfer between TMP and SAZn@BC.

### 2.7. Density functional theory (DFT) calculations

Molecular simulations were performed using DFT in Gaussian16 utilizing the M06L function.<sup>20</sup> The 6-31G\* basis set was chosen for C, N, H, and O, while LANL2DZ was used for Zn atoms. The implicit solvent model of solvation based on density (SMD)<sup>21</sup> was employed to describe water solvation in all simulations. The initial model of SAZn@BC was built using 10 conjugated six-member rings with four center rings doped with one N each and coordinated with a zinc atom in the center (Fig. S2†). Hydroquinone and quinone were attached on the side as representative oxygen functional groups in the biochar support. To elucidate the role of Zn single atoms, simulations were also performed with the BC control containing 0.0 wt% of Zn. Species O<sub>2</sub>, <sup>•</sup>OOH, and H<sub>2</sub>O<sub>2</sub> were optimized on the surface of the catalyst as higher multiplicities were also investigated to find lower energy configuration. Frequency calculation was performed at *T* = 298 K and *P* = 1 atm using harmonic potential approximation after optimization of the structures. The population analysis was performed by the Natural Bond Orbital (NBO) method.

### 2.8. Recyclability study

After each run, the SAZn@BC was collected with a 0.45 μm membrane filter and washed with 200 mL ultrapure water. It was then regenerated by heating at either 100 °C or 250 °C for 5.0 hours or dried at room temperature (25 °C) for 48 hours. After drying, the biochar was used directly in TMP degradation without additional treatments. The heating regeneration was repeated after the second cycle to evaluate the long-term reusability of the catalyst. In each cycle, the recovery rate was about 90% due to the incomplete recovery of SAZn@BC adsorbed on the membrane. However, this did not affect the assessment of the performance of the regenerated SAZn@BC in our study because plenty of replicates were prepared so that the regenerated SAZn@BC used in each replicate was the same as the pristine SAZn@BC.

## 3. Results and discussion

### 3.1 Characterization of the single-atom Zn catalyst supported on biochar

The XRD pattern of SAZn@BC in Fig. 1(a) had an almost flat curve indicating the successful removal of ZnO. The fitting result of the N 1s spectrum of XPS analysis in Fig. 1(b) supports the formation of the Zn–N–C bond by the Zn–N peak at 400.12 eV.<sup>22</sup> The peaks at 401.06 eV, 399.11 eV, and 398.02 eV belong to graphitic N, pyrrolic N and pyridinic N, respectively,<sup>22</sup> indicating the formation of N-doped carbon. The strong peak at 284.43 eV in the C 1s spectrum (Fig. 1(c)) indicates the dominance of aromatic carbon in SAZn@BC.<sup>23</sup> Strong peaks at 286.51 eV and 288.11 eV in the C 1s spectrum correspond to C–O/C–N and C=O/C=N peaks,<sup>24</sup> respectively, confirmed by the peaks at 531.18 eV and 533.30 eV in the O 1s spectrum (Fig. 1(d)).<sup>25</sup> The strong C–O peaks could be attributed to the presence of phenolic and hydroquinone groups<sup>26,27</sup> while the intensive C=O peaks suggest the presence of the quinone moiety on the catalyst.<sup>11,28</sup>

HAADF-TEM analysis was also performed (Fig. 1). The presence of Zn single-atom sites, represented by the bright dots with a diameter of around 2 Å, can be clearly seen in Fig. 1(e), and no aggregation was observed. The EDS mapping (Fig. 1(f)–(i)) in the highlighted area in Fig. 1(e) shows the ultrafine distribution of C, N, Zn, and O atoms with a composition of 80.72, 12.18, 0.83, and 6.22 wt% in SAZn@BC, respectively. XAFS results that reveal the local coordination environment of Zn atoms in SAZn@BC agree with the TEM observation in Fig. 1(j)–(l). According to the normalized Zn K-edge X-ray absorption near edge structure (XANES) spectra of SAZn@BC, Zn metal, and ZnO in Fig. 1(j), the valence state of Zn in SAZn@BC is +2. The EXAFS spectrum was analyzed to gain information on the coordination environment of Zn atoms on biochar. The Fourier transformed EXAFS result (Fig. 1(k)) shows that Zn in SAZn@BC has a prominent peak at around 1.58 Å, corresponding to the Zn–N bond.<sup>13,30,31</sup> The absence of the Zn–Zn peak at 2.30 Å indicates that all Zn atoms in SAZn@BC are in single-atom form. To further reveal the local coordination structure, Fourier-transformed EXAFS data were fitted by Artemis software,



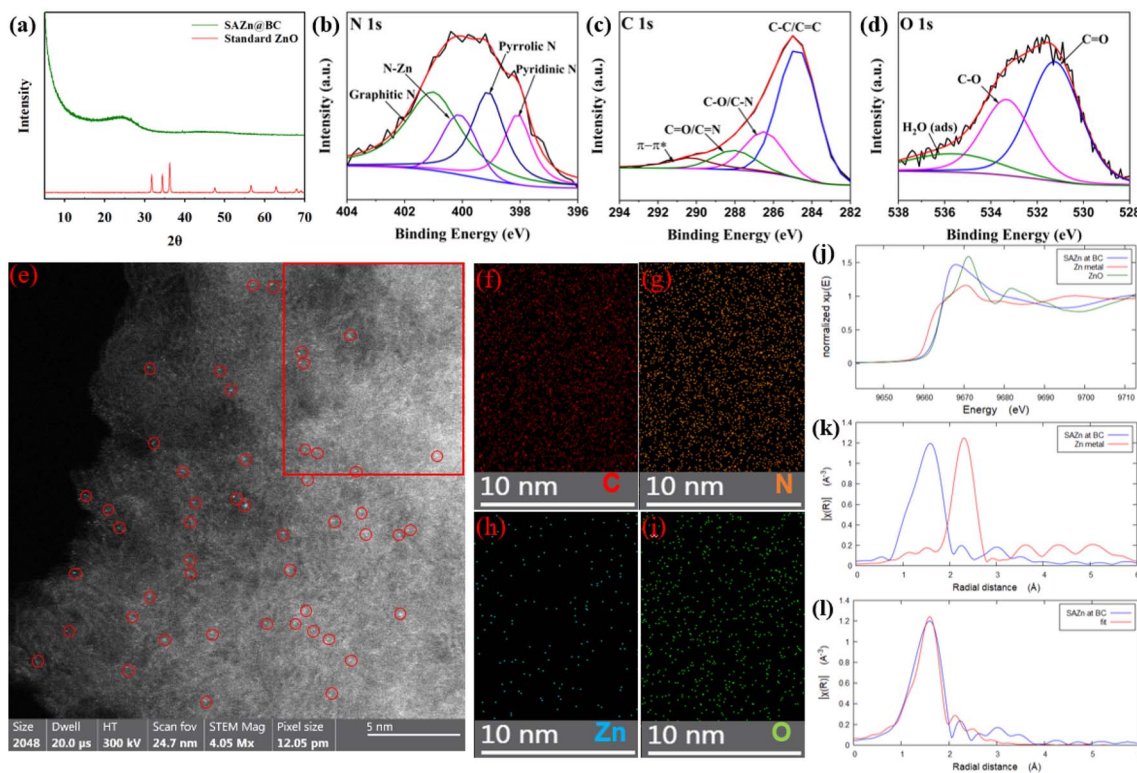


**Fig. 1** (a) X-ray diffraction (XRD) patterns of SAZn@BC and standard ZnO.<sup>29</sup> XPS spectra of N 1s (b), C 1s (c), and O 1s (d) of SAZn@BC. (e) High-angle annular dark field transmission electron microscopy (HAADF-TEM) image of SAZn@BC. Red circles mark the location of zinc single atoms. (f–i) Elemental mapping images of the SAZn@BC for C, N, Zn, and O, respectively in the highlighted red box region of (e). (j) Normalized Zn K-edge XANES spectrum of SAZn@BC, Zn foil, and ZnO. (k) Fourier transformed EXAFS spectrum of SAZn@BC and Zn foil. (l) EXAFS fitting with a Zn–N<sub>4</sub> model.

which indicates that every Zn atom in SAZn@BC is linked to 4 N (Zn–N<sub>4</sub> structure) with a mean bond length of 2.07 Å (Fig. 1(l)).

### 3.2. Removal of TMP by the single-atom Zn catalyst supported on biochar

At a dosage of 0.2 g L<sup>-1</sup>, single-atom Zn biochar (SAZn@BC) with 1 wt% Zn by weight removed 74.0% TMP in 10 hours without any additional chemical agents, and an increase of SAZn@BC at 0.4 g L<sup>-1</sup> achieved a remarkable 98.0% removal of TMP in 30 min (Fig. 2(a)). Previous studies on single-atom metal catalysts almost exclusively focused on activating

peroxymonosulfate/peroxydisulfate in sulfate radical-based advanced oxidation processes to achieve contaminant removal.<sup>32–34</sup> This is the first time that it has been shown that SAZn@BC alone can result in significant contaminant removal. While adsorption might play an important role in the beginning, the enabled degradation of TMP by SAZn@BC was likely the main reason for the excellent performance of SAZn@BC, which was confirmed by the detection of various TMP metabolites from bond cleavage, demethylation and hydrolysis with an untargeted analysis (Fig. S3†). In addition, the TOC measurement (Fig. 2(c)) also suggested the increased TOC

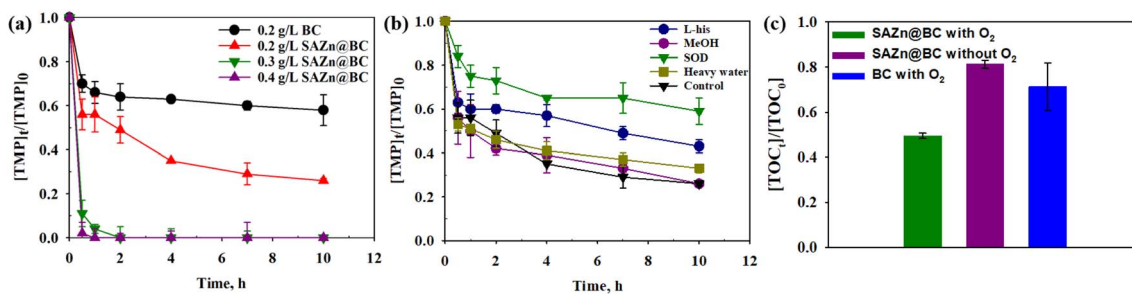


**Fig. 2** (a) Removal efficiency of TMP by SAZn@BC at different dosages (BC as control). (b) The degradation of TMP by SAZn@BC with different quenchers. (c) TOC removal by SAZn@BC and BC in normal or deoxygenated water. Reaction conditions: running time = 10 hours, [TMP]<sub>0</sub> = 10 μM, [biochar] = 0.2 g L<sup>-1</sup>, [L-His] = 10.0 μM, [MeOH] = 0.5 M, [SOD] = 50.0 U mL<sup>-1</sup>, [pH] = 4.3, T = 25.0 °C.



removal from around 30% to 50% with the incorporation of single-atom Zn into the biochar. Interestingly, the performance of SAZn@BC depended heavily on the levels of dissolved oxygen (DO), Fig. S5,<sup>†</sup> suggesting that DO or reactive oxygen species (ROS) might play a significant role in the degradation of TMP by SAZn@BC. The TOC study also suggested the important role of DO in the system in that the TOC removal decreased from 50% to 20% after the deoxygenation.

### 3.3 Quenching study and TMP degradation by reactive species

Based on the results in Fig. 2(b), MeOH did not affect the degradation of TMP, suggesting that the hydroxyl radical ( $\cdot\text{OH}$ ) was not involved in TMP degradation by ZnSA@BC. L-His

significantly inhibited the TMP degradation. However, replacing ultrapure water with  $\text{D}_2\text{O}$  did not lead to enhanced TMP removal, suggesting a minimal role of  $^1\text{O}_2$  because  $^1\text{O}_2$  has a longer lifetime in  $\text{D}_2\text{O}$  and would lead to a greater TMP removal if it was involved in TMP degradation.<sup>35</sup> After the addition of low-concentration superoxide dismutase (SOD), TMP degradation dropped from 74.0% to 41.0%. This strong inhibition implied the critical role of  $\text{O}_2^{\cdot-}$ , and the generation was further confirmed by the NBT test (Fig. S6<sup>†</sup>).

However,  $\text{O}_2^{\cdot-}$  has a low redox potential of  $E^0 = -0.33\text{ V}$  (vs. NHE)<sup>36</sup> and is unlikely to oxidize TMP ( $E^0 = +1.1\text{ V}$  (vs. NHE)).<sup>37</sup> In an acidic environment (pH 4.3), the majority of  $\text{O}_2^{\cdot-}$  is in the form of hydroperoxyl radical ( $\cdot\text{OOH}$ ) ( $E^0 = +1.44\text{ V}$  (vs. NHE),  $\text{p}K_{\text{a}} = 4.88$ ) which is a much stronger oxidant.  $\cdot\text{OOH}$  could further

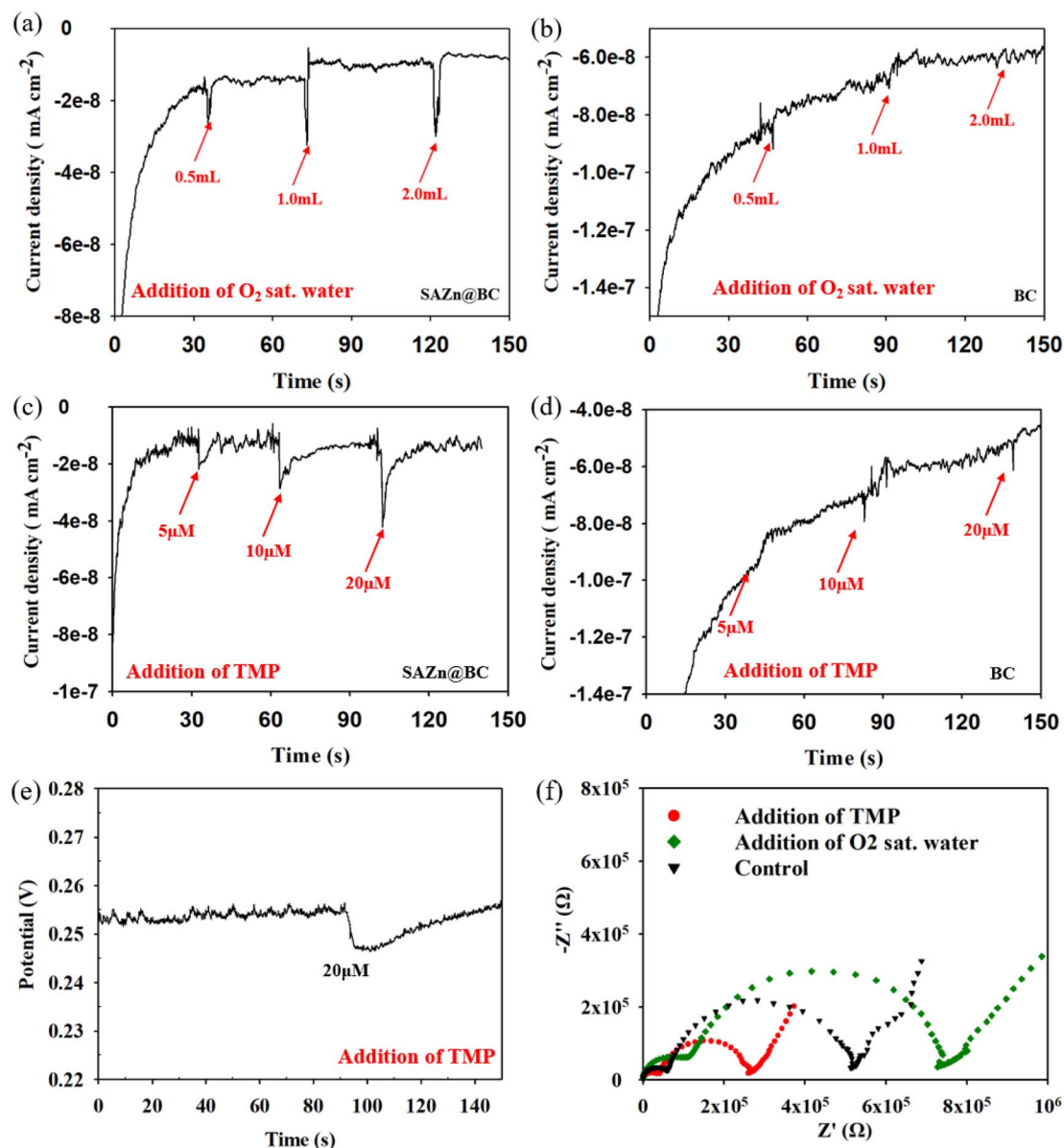


Fig. 3 The chronoamperometry  $i-t$  curves of catalyst suspension. (a and b) Deoxygenated water with SAZn@BC and BC after the addition of different volumes of oxygen-saturated water, (c and d) typical deionized water with SAZn@BC and BC after the addition of different concentrations of TMP, (e) open circuit potential measurements of SAZn@BC after the addition of TMP and (f) Nyquist plots of electrochemical impedance spectra.



produce  $\text{H}_2\text{O}_2$  ( $E^0 = +1.8 \text{ V}$  (vs. NHE)), as shown in reactions R1 to R4 (Fig. S7†).<sup>35</sup> And reactions between  $\text{H}_2\text{O}_2$ ,  $\cdot\text{OOH}$  and TMP were proposed as the main mechanisms leading to the indirect oxidation of TMP by SAZn@BC. The UV-vis measurements suggested that  $\text{H}_2\text{O}_2$  concentration was about 0.05 mM in our system at the time of measurement (Fig. S8†). The electron transfer from SAZn@BC to DO was also confirmed by chronoamperometry  $I-t$  measurement, Fig. 3(a), with the current change intensity proportional to the amount of  $\text{O}_2$  added to the system. Importantly, this result was not found in the BC system, Fig. 3(b), indicating the necessity of single-atom Zn as an electron transfer bridge to facilitate electron transfer.

### 3.5 Direct TMP oxidation by the single-atom Zn catalyst on biochar support

Although TMP degradation by ROS was significant (*i.e.*, 38.0–41.0%), yet TMP in the system was still removed after SOD quenching, suggesting that additional mechanisms might be occurring. Adsorption on the biochar support material likely contributed to part of the removal of TMP from solution. Chronoamperometry measurements revealed the positive and linear correlation ( $R^2 = 0.93$ ) of the current change intensity with the concentration of TMP added to the system (Fig. 3(c)), confirming direct electron transfer between SAZn@BC and TMP,<sup>38,39</sup> which was not found in the BC system, Fig. 3(d), again emphasizing the important role of single-atom Zn sites for the direct oxidation of TMP. The direct electron transfer was also supported by the OCP measurements, Fig. 3(e), that showed a signal drop after the addition of TMP, indicating its direct oxidation.<sup>40</sup> The EIS Nyquist plots, Fig. 3(f), revealed different electron transfer resistance of the SAZn@BC after TMP addition, providing further support of direct electron transfer between TMP and SAZn@BC. Overall, our results demonstrate a combined radical pathway and direct oxidation for TMP degradation by SAZn@BC as illustrated in Fig. 4.

### 3.6 DFT calculations

The lowest energy values of different multiplicities were employed for binding free energy calculations and the results

are tabulated in Fig. S9.† The negative binding-free energy indicated that  $\text{O}_2$  and  $\cdot\text{OOH}$  can be easily adsorbed on the catalyst surface to induce reactions to generate  $\text{O}_2^{\cdot-}$  and  $\text{H}_2\text{O}_2$ .<sup>41</sup> The overall reaction potentials of R1, R3, and R4 (Fig. S7†) are summarized in Table S1.† The calculation of free energy with respect to the biased potential was performed using the computational hydrogen electrode model.<sup>42</sup> Here, the bias potential  $U$  (V) denotes the voltage applied to an electrode in an electrochemical cell relative to a reference electrode. In the model, the free energy ( $\Delta G$ ) was defined as  $eU$  with a unit of eV.<sup>43</sup> The reactions of  $\text{O}_2$  and  $\cdot\text{OOH}$  accepting electrons from SAZn@BC to generate  $\text{O}_2^{\cdot-}$  and  $\text{H}_2\text{O}_2$  were simulated at  $U = 0 \text{ V}$ , implying that no voltage was applied to the system, and the negative free energy of  $-1.70$ ,  $-1.91$  and  $-1.4 \text{ eV}$  for reactions R1, R3 and R4 demonstrated that these reactions are spontaneous. DFT calculations were also performed for the catalyst without Zn (Table S2†). After eliminating Zn, the free energy of R1 for the generation of  $\text{O}_2^{\cdot-}$  turned positive ( $+0.48 \text{ eV}$ ), suggesting the necessity of the Zn single-atom sites for the spontaneous ROS generation. The results agree with the poor TOC removal in the reactor with BC control (Fig. 2(c)).

The results of NBO calculations for the catalyst indicate the direction of electron transfer between reactants and SAZn@BC (Table S3†). Positive values for SAC/ $\text{O}_2$  and SAC/ $\cdot\text{OOH}$  indicate electron transfer from the hydroquinone to  $\text{O}_2$  and  $\cdot\text{OOH}$ . The negative values for SAC/TMP revealed the opposite electron transfer. Overall, DFT calculations supported our experimental studies that  $\text{O}_2$  and  $\cdot\text{OOH}$  are reduced while TMP is oxidized by SAZn@BC, leading to effective degradation of TMP through both pathways. A comparison of the degradation rate constant of TMP, Table S4,† showed that even though SAZn@BC did not display the highest performance among all catalysts, it had much higher TMP removal efficiency than conventional photocatalysts or biochar products. However, it is important to emphasize that this study was performed in deionized water. Natural water contains a diverse group of constituents such as inorganic anions which are known to quench some reactive oxygen species and form secondary radicals. We examined the impact of several common anions such as  $\text{PO}_4^{3-}$  and  $\text{CO}_3^{2-}$  on the removal of TMP by SAZn@BC (Fig. S10†). All inorganic anions inhibited the removal of TMP, with  $\text{CO}_3^{2-}$  demonstrating the greatest inhibition. These results suggest that the composition of natural water has a marked impact on the performance of SAZn@BC and additional studies are needed to gain more insights into the potential effectiveness of SAZn@BC in natural water.

## 4. Reusability

The reusability of a catalyst is an important consideration in sustainable applications of catalysts. Unfortunately, a significant drop in performance was noticed for the SAZn@BC air-dried after reaction with TMP (Fig. S11(a)†). The change of the catalyst surface chemical structure could be one of the reasons for the performance decline. A comparison of the O 1s spectrum of XPS showed a substantial decrease of the C–O bond at 533.30 eV and an increase of C=O at 531.18 eV after the

### Oxidation by Reactive Species      Direct Oxidation

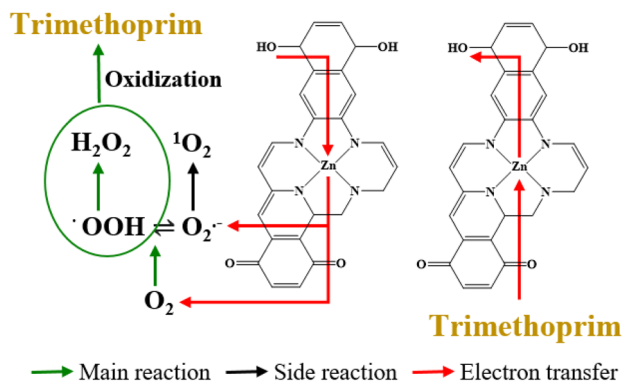


Fig. 4 Schematic illustration of the TMP degradation pathways by SAZn@BC.



reaction (Fig. S12†). This change was also supported by the C 1s spectrum, likely from the consumption of phenolic groups and transformation of hydroquinone to quinone moieties.<sup>11</sup> The blockage of micropores and active sites by undegraded TMP could be another reason for the reduced performance of SAZn@BC. Interestingly, simple heating at 100 °C and 250 °C significantly improved the catalytic performance of SAZn@BC to a level comparable to the original catalyst. Unfortunately, after one cycle of heating, SAZn@BC regenerated at 100 °C showed poor performance even after heating at the same temperature again (Fig. S11(b)†). This may be due to the carbonization of TMP on the surface. However, SAZn@BC regenerated at 250 °C roughly maintained its efficacy for TMP removal after the second heating, suggesting that high temperature heating might be a simple but effective approach to regenerate the catalyst. This is attributed to the fact that the higher temperature favors the formation of redox active phenolic and hydroquinone moieties on biochar,<sup>15</sup> a critical factor in the catalytic function of SAZn@BC as discussed above. Further studies on the stability of single atom sites during chemical reactions and their regeneration mechanisms are needed to advance the applications of single atom metal catalysts on a biochar support in environmental applications.

## 5. Conclusions

Our study demonstrated the successful synthesis of a single-atom Zn catalyst supported on biochar with a Zn–N<sub>4</sub> coordination structure. The catalyst alone led to significant TMP degradation *via* co-occurring radical reaction and direct oxidation, which could lead to more efficient environmental applications of SACs. The electrocatalytic performance of the catalyst could be attributed to the coordination between redox active functional groups and zinc single-atom sites. Direct TMP oxidation was enabled by the electron transfer from TMP to SAZn@BC. And the electron transfer from the SAZn@BC to dissolved oxygen generates H<sub>2</sub>O<sub>2</sub> and <sup>•</sup>OOH, leading to the radical pathway of TMP degradation. All these reactions and electron transfer pathways were mediated by single-atom Zn sites and verified by DFT calculations. The cost-effectiveness of SAZn@BC and its simple regeneration makes SAZn@BC alone a highly effective and sustainable material in environmental remediation. Notably, tremendous amounts of natural biomass contain transition heavy metals, and the disposal of this biomass has been a main environmental challenge. Our research offers an appealing approach to upcycle metal-bearing biomass by converting it into effective metal catalysts on a carbon support.

## Author contributions

All authors contributed to the study conception and analysis. Material preparation, data collection and analysis were performed by Jieming Yuan and Yunkyong Han. Krishnamoorthy Sathiyam contributed to the electrochemical analysis. Abdol Hadi Mokarizadeh and Mesfin Tsige conducted the DFT calculations. Jiechao Jiang performed the XPS analysis. Virender Sharma and Xingmao Ma supervised the studies. The first

draft was written by Jieming Yuan and all authors commented on the manuscript. All authors read and approved the final version of the manuscript.

## Conflicts of interest

The authors have no relevant financial or nonfinancial competing interests to disclose.

## Acknowledgements

This work was partially supported by the Water Excellence Seed Grant from Texas Water Resources Institute to Xingmao Ma and Virender Sharma.

## References

- 1 A. Ikhlaq, D. R. Brown and B. Kasprzyk-Hordern, Catalytic ozonation for the removal of organic contaminants in water on alumina, *Appl. Catal., B*, 2015, **165**, 408–418.
- 2 S. Rojas and P. Horcajada, Metal–organic frameworks for the removal of emerging organic contaminants in water, *Chem. Rev.*, 2020, **120**, 8378–8415.
- 3 S. Shrestha, B. Wang and P. Dutta, Nanoparticle processing: understanding and controlling aggregation, *Adv. Colloid Interface Sci.*, 2020, **279**, 102162.
- 4 J. Liu, Y. Zou, D. Cruz, A. Savateev, M. Antonietti and G. Vilé, Ligand–metal charge transfer induced *via* adjustment of textural properties controls the performance of single-atom catalysts during photocatalytic degradation, *ACS Appl. Mater. Interfaces*, 2021, **13**, 25858–25867.
- 5 D. B. Miklos, C. Remy, M. Jekel, K. G. Linden, J. E. Drewes and U. Hübner, Evaluation of advanced oxidation processes for water and wastewater treatment—A critical review, *Water Res.*, 2018, **139**, 118–131.
- 6 Y. Shang, X. Xu, B. Gao, S. Wang and X. Duan, Single-atom catalysis in advanced oxidation processes for environmental remediation, *Chem. Soc. Rev.*, 2021, **50**, 5281–5322.
- 7 J. Cao, L. Lai, B. Lai, G. Yao, X. Chen and L. Song, Degradation of tetracycline by peroxymonosulfate activated with zero-valent iron: performance, intermediates, toxicity and mechanism, *Chem. Eng. J.*, 2019, **364**, 45–56.
- 8 X. Wu and J.-H. Kim, Outlook on single atom catalysts for persulfate-based advanced oxidation, *ACS ES&T Eng.*, 2022, **2**, 1776–1796.
- 9 C. Gao, J. Low, R. Long, T. Kong, J. Zhu and Y. Xiong, Heterogeneous single-atom photocatalysts: fundamentals and applications, *Chem. Rev.*, 2020, **120**, 12175–12216.
- 10 M. B. Gawande, P. Fornasiero and R. Zbořil, Carbon-based single-atom catalysts for advanced applications, *ACS Catal.*, 2020, **10**, 2231–2259.
- 11 J. Yuan, Y. Wen, D. D. Dionysiou, V. K. Sharma and X. Ma, Biochar as a novel carbon-negative electron source and mediator: electron exchange capacity (EEC) and environmentally persistent free radicals (EPFRs): a review, *Chem. Eng. J.*, 2021, 132313.



- 12 N. Wang, Z. Liu, J. Ma, J. Liu, P. Zhou, Y. Chao, *et al.*, Sustainability perspective-oriented synthetic strategy for zinc single-atom catalysts boosting electrocatalytic reduction of carbon dioxide and oxygen, *ACS Sustainable Chem. Eng.*, 2020, **8**, 13813–13822.
- 13 J. Li, S. Chen, N. Yang, M. Deng, S. Ibraheem, J. Deng, *et al.*, Ultrahigh-loading zinc single-atom catalyst for highly efficient oxygen reduction in both acidic and alkaline media, *Angew. Chem., Int. Ed.*, 2019, **58**, 7035–7039.
- 14 E. Grilla, J. Vakros, I. Konstantinou, I. D. Manariotis and D. Mantzavinos, Activation of persulfate by biochar from spent malt rootlets for the degradation of trimethoprim in the presence of inorganic ions, *J. Chem. Technol. Biotechnol.*, 2020, **95**, 2348–2358.
- 15 Q. Wang, W. Pang, Y. Mao, Q. Sun, P. Zhang, Q. Ke, *et al.*, Study of the degradation of trimethoprim using photo-Fenton oxidation technology, *Water*, 2019, **11**, 207.
- 16 Z. Cetecioglu, B. Ince, D. Orhon and O. Ince, Anaerobic sulfamethoxazole degradation is driven by homoacetogenesis coupled with hydrogenotrophic methanogenesis, *Water Res.*, 2016, **90**, 79–89.
- 17 M. Newville, IFEFFIT: interactive XAFS analysis and FEFF fitting, *J. Synchrotron Radiat.*, 2001, **8**, 322–324.
- 18 H. Goto, Y. Hanada, T. Ohno and M. Matsumura, Quantitative analysis of superoxide ion and hydrogen peroxide produced from molecular oxygen on photoirradiated TiO<sub>2</sub> particles, *J. Catal.*, 2004, **225**, 223–229.
- 19 R. F. P. Nogueira, M. C. Oliveira and W. C. Paterlini, Simple and fast spectrophotometric determination of H<sub>2</sub>O<sub>2</sub> in photo-Fenton reactions using metavanadate, *Talanta*, 2005, **66**, 86–91.
- 20 Y. Zhao and D. G. Truhlar, A new local density functional for main-group thermochemistry, transition metal bonding, thermochemical kinetics, and noncovalent interactions, *J. Chem. Phys.*, 2006, **125**, 194101.
- 21 A. V. Marenich, C. J. Cramer and D. G. Truhlar, Universal solvation model based on solute electron density and on a continuum model of the solvent defined by the bulk dielectric constant and atomic surface tensions, *J. Phys. Chem. B*, 2009, **113**, 6378–6396.
- 22 M. Tong, F. Sun, Y. Xie, Y. Wang, Y. Yang, C. Tian, *et al.*, Operando cooperated catalytic mechanism of atomically dispersed Cu-N<sub>4</sub> and Zn-N<sub>4</sub> for promoting oxygen reduction reaction, *Angew. Chem., Int. Ed.*, 2021, **60**, 14005–14012.
- 23 H. Wang, Y. Wang, Y. Li, X. Lan, B. Ali and T. Wang, Highly efficient hydrogenation of nitroarenes by N-doped carbon-supported cobalt single-atom catalyst in ethanol/water mixed solvent, *ACS Appl. Mater. Interfaces*, 2020, **12**, 34021–34031.
- 24 H. Fan, H. Yu, Y. Zhang, Y. Zheng, Y. Luo, Z. Dai, *et al.*, Fe-doped Ni<sub>3</sub>C nanodots in N-doped carbon nanosheets for efficient hydrogen-evolution and oxygen-evolution electrocatalysis, *Angew. Chem., Int. Ed.*, 2017, **56**, 12566–12570.
- 25 H. Idriss, On the wrong assignment of the XPS O1s signal at 531–532 eV attributed to oxygen vacancies in photo- and electro-catalysts for water splitting and other materials applications, *Surf. Sci.*, 2021, **712**, 121894.
- 26 F. J. Chacón, M. L. Cayuela, A. Roig and M. A. Sánchez-Monedero, Understanding, measuring and tuning the electrochemical properties of biochar for environmental applications, *Rev. Environ. Sci. Biotechnol.*, 2017, **16**, 695–715.
- 27 S. Li, L. Shao, H. Zhang, P. He and F. Lü, Quantifying the contributions of surface area and redox-active moieties to electron exchange capacities of biochar, *J. Hazard. Mater.*, 2020, **394**, 122541.
- 28 L. Klüpfel, M. Keilueit, M. Kleber and M. Sander, Redox properties of plant biomass-derived black carbon (biochar), *Environ. Sci. Technol.*, 2014, **48**, 5601–5611.
- 29 W. Frank, *Powder Diffraction File for Inorganic Phase*, International Center for Diffraction Data, Philadelphia, 1981.
- 30 F. Yang, P. Song, X. Liu, B. Mei, W. Xing, Z. Jiang, *et al.*, Highly efficient CO<sub>2</sub> electroreduction on ZnN<sub>4</sub>-based single-atom catalyst, *Angew. Chem., Int. Ed.*, 2018, **57**, 12303–12307.
- 31 L. Han, S. Song, M. Liu, S. Yao, Z. Liang, H. Cheng, *et al.*, Stable and efficient single-atom Zn catalyst for CO<sub>2</sub> reduction to CH<sub>4</sub>, *J. Am. Chem. Soc.*, 2020, **142**, 12563–12567.
- 32 L. Zhang, X. Jiang, Z. Zhong, L. Tian, Q. Sun, Y. Cui, *et al.*, Carbon nitride supported high-loading Fe single-atom catalyst for activation of peroxymonosulfate to generate <sup>1</sup>O<sub>2</sub> with 100% selectivity, *Angew. Chem., Int. Ed.*, 2021, **60**, 21751–21755.
- 33 T. Yang, S. Fan, Y. Li and Q. Zhou, Fe-N/C single-atom catalysts with high density of Fe-N<sub>x</sub> sites toward peroxymonosulfate activation for high-efficient oxidation of bisphenol A: electron-transfer mechanism, *Chem. Eng. J.*, 2021, **419**, 129590.
- 34 Y. Xue, N. N. T. Pham, G. Nam, J. Choi, Y.-Y. Ahn, H. Lee, *et al.*, Persulfate activation by ZIF-67-derived cobalt/nitrogen-doped carbon composites: kinetics and mechanisms dependent on persulfate precursor, *Chem. Eng. J.*, 2021, **408**, 127305.
- 35 Y. Wen, C.-H. Huang, D. C. Ashley, D. Meyerstein, D. D. Dionysiou, V. K. Sharma, *et al.*, Visible light-induced catalyst-free activation of peroxydisulfate: pollutant-dependent production of reactive species, *Environ. Sci. Technol.*, 2022, **56**, 2626–2636.
- 36 J. Ma, Z. Wei, R. Spinney, D. D. Dionysiou and R. Xiao, Emerging investigator series: could the superoxide radical be implemented in decontamination processes?, *Environ. Sci.*, 2021, **7**, 1966–1970.
- 37 H. da Silva, J. G. Pacheco, J. M. C. S. Magalhães, S. Viswanathan and C. Delerue-Matos, MIP-graphene-modified glassy carbon electrode for the determination of trimethoprim, *Biosens. Bioelectron.*, 2014, **52**, 56–61.
- 38 Z. Li, K. Li, S. Ma, B. Dang, Y. Li, H. Fu, *et al.*, Activation of peroxymonosulfate by iron-biochar composites: comparison of nanoscale Fe with single-atom Fe, *J. Colloid Interface Sci.*, 2021, **582**, 598–609.
- 39 S. Cai, X. Zuo, H. Zhao, S. Yang, R. Chen, L. Chen, *et al.*, Evaluation of N-doped carbon for the peroxymonosulfate



- activation and removal of organic contaminants from livestock wastewater and groundwater, *J. Mater. Chem. A Mater.*, 2022, **10**, 9171–9183.
- 40 M. Yang, Z. Hou, X. Zhang, B. Gao, Y. Li, Y. Shang, *et al.*, Unveiling the origins of selective oxidation in single-atom catalysis *via* Co–N<sub>4</sub>–C intensified radical and nonradical pathways, *Environ. Sci. Technol.*, 2022, **56**, 11635–11645.
- 41 Z. Wang, W. Wang, J. Wang, D. Wang, M. Liu, Q. Wu, *et al.*, Single-atom catalysts with ultrahigh catalase-like activity through electron filling and orbital energy regulation, *Adv. Funct. Mater.*, 2023, **33**, 2209560.
- 42 J. K. Nørskov, J. Rossmeisl, A. Logadottir, L. Lindqvist, J. R. Kitchin, T. Bligaard, *et al.*, Origin of the overpotential for oxygen reduction at a fuel-cell cathode, *J. Phys. Chem. B*, 2004, **108**, 17886–17892.
- 43 A. Kulkarni, S. Siahrostami, A. Patel and J. K. Nørskov, Understanding catalytic activity trends in the oxygen reduction reaction, *Chem. Rev.*, 2018, **118**, 2302–2312.

